Spontaneous Emission Rate Enhancement of Silicon Nanocrystals by Plasmonic Bandgap on Copper Grating

Xue Feng, Fang Liu, and Yidong Huang, *Member, IEEE*

***Abstract*—The spontaneous emission (SE) rate enhancement due to surface plasmon polariton bandgap effect on copper grating was evaluated by calculating the dispersion relation and the electromagnetic field distribution simultaneously. Within the frequency range of silicon nanocrystals (Si-NC) luminescence ($\hbar\omega = 1.6$ eV–1.9 eV), the calculated maximum averaged Purcell factors is about 30–163 for sinusoidal shaped Cu-Si_3 N_4 grating. It is proved that copper can be adopted to enhance the SE of Si-NCs. Since copper is the most commonly adopted metal for silicon integrated-circuit manufacturing, such results pave a promising way for integrating Si emitters on microelectronics chips.**

***Index Terms*—Band gap, copper, metallic grating, spontaneous emission, surface plasmon polariton.**

I. Introduction

SILICON light emitters are very promising for optical interconnection or other applications [1]–[7] because of their compatibility with silicon integrated-circuit (IC) manufacturing. Generally, bulk silicon has been considered unsuitable for optoelectronic applications due to its indirect electronic bandgap. Recently, there has been much effort on improving the light-emission properties of silicon such as porous silicon [3], [8], erbium doped silicon [9], all-silicon Raman laser [10] and silicon nanocrystals (Si-NC) [4]–[7]. Among them, Si-NC has attracted a great interest since intense visible luminescence has been observed at room temperature due to quantum confinement effect [3]–[7]. Moreover, stimulated emission and light amplification in Si-NCs have also been observed [1]. However, the internal quantum efficiency of light emission from Si-NC is still not high enough for real applications due to dominant nonradiative recombination. Surface plasmon polariton (SPP) is an attractive candidate to solve such long-standing obstacle [11]–[16]. Metal SPP enhanced spontaneous emission (SE) rate has been proposed and demonstrated on wide bandgap semiconductors, such as GaN/InGaN [11]–[14] and ZnO [15]. Unfortunately, this method is not so effective for light emission from Si-NCs. Unless the average size of Si-NC is very small, the central luminescent frequencies are usually much lower than the plasmon frequency of common metals, e.g., gold (Au), silver (Ag), copper (Cu), and aluminum (Al). In order to apply metal SPP enhancement for Si emitter, the plasmon frequency should be engineered to match the luminescence of Si-NCs. Up to now, there are two approaches that have been reported. One is based on a metal-rich Au (1-α)-SiO_2 (α) cermet nanowaveguide proposed in our previous work [17]. By properly choosing the component of the cermet, the SPP-like dispersion of the nanowaveguide can be engineered so that the SE is greatly enhanced. Another is based on metallic nanostructures, e.g., metallic gratings or islands/particles. In [18], Y. Gong, *et al.* have been proposed and demonstrated that the SPP enhancement can be achieved with Au-gratings fabricated on the top of Si-NC embedded in silicon dioxide. Furthermore, our recent work has proved that not only Au, but also Ag and Al, which SPP resonance frequencies are rather higher, can be adopted to enhance the SE from Si-NCs [19]. In [20], [21], J. S. Bitten, *et al.* have experimentally reported that nanoporous Au layer and Ag nanoparticles array can be applied to achieve plasmon-enhanced photoluminescence of Si-NCs.

It should be noticed that Au and Ag are preferred metal materials in these previous works [17]–[21]. The reason is based on the facts that Au is a kind of metal with stable chemical characteristic and the loss of Ag in visible-light region is the lowest compared to other metals. However, it is well known that Cu, rather than Au and Ag, is the mainstay metal material in microelectronics chips. If Cu can be adopted to provide SPP enhancement of light emission from Si emitters, it would be a notable promotion for integrating Si emitters on microelectronics chip.

In this paper, the SE rate enhancement due to SPP bandgap (SPPBG) effect on Cu-Si_3N_4 grating is evaluated by Purcell factor (PF). For PF calculation, both dispersion relation and electromagnetic field distribution of SPP mode are essential. As discussed in our previous work [22], the Green' function method (GFM) based on Rayleigh expansion, which is widely adopted to investigate the SPP scattering problem, is hard to be used to calculate the electromagnetic field distribution in treating the homogeneous problem, even the dispersion relation of SPP mode can be well obtained. While Chandezon's approach (CDA), which is superior to Rayleigh expansion method for constructing the electromagnetic field distribution in two-dimensional expansion form, can not be used to calculate the dispersion relation. In order to obtain the full SPP mode solution including both of dispersion relation and field distribution, we demonstrate a combination method to obtain the numerical

Manuscript received October 14, 2009; revised January 10, 2010; accepted February 02, 2010. First published February 17, 2010; current version published April 30, 2010. This work was supported in part by the National Basic Research Program of China (973 Program) under Contract 2007CB307004 and National Natural Science Foundation of China under Contract NSFC-60877023.

The authors is with State Key Laboratory of Integrated Optoelectronics, Department of Electronic Engineering, Tsinghua University, Beijing 100084, China (e-mail: x-feng@tsinghua.edu.cn; yidonghuang@tsinghua.edu.cn).

Digital Object Identifier 10.1109/JLT.2010.2042788

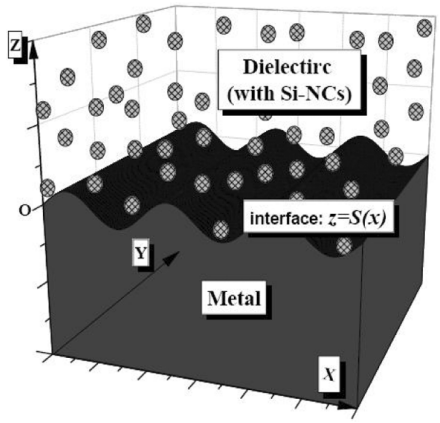

Fig. 1. Schematic cylindrical periodic dielectric-metal interface and reference coordinate system. The interface consists of dielectric in the region $z > s(x)$ and metal in the region $z < s(x)$.

solution of SPP mode propagating on a one dimensional (1-D) metallic grating by taking the advantages of GFM and CDA [22]. Comparing to the two dimensional FDTD simulation used in [18], our proposed method is time-cost effective and stable since only moderate frequency step and coefficients matrix order are required to reach sufficient accuracy. After obtaining both the dispersion relation $k(\omega)$ and the electromagnetic field distribution $\boldsymbol{E}(x,z)$, we deduce a set of new formulations for calculating SE rate and PF on such 1-D metallic grating from Fermi's Golden Rule and calculate the PFs for various Cu-Si_3N_4 grating periods. The calculation results show that, with proper grating period, the band edge (BE) frequency of Cu-Si_3N_4 grating can be varied within the frequency range of Si-NCs luminescence ($\hbar\omega = 1.9$ eV–1.6 eV). Consequently, significant SE enhancement can be achieved at the BE-frequency. The maximum PFs for Cu-Si_3N_4 gratings with 1 μm width are as high as 162.7–29.8. This is promising to be used to enhance the luminescence of Si light emitter, especially for the application of optical interconnection on chip.

This paper is organized as followed. In Section II, the considered theoretical model and calculation approach are described. In Section III, the calculated results of Cu-Si $_3N_4$ interface with sinusoidal shape are presented. In Section IV, the results for Cu-Si_3N_4 grating are discussed with Au, Ag and Al- Si $_3N_4$ gratings. The characteristics of SE enhancement at different BE-frequency are compared and discussed. Finally, it is also discussed how to achieve maximum SE enhancement. Section V provides a summary.

II. Theoretical Model and Approach

A. Theoretical Model

As shown in Fig. 1, the shape of spatially periodic metal-dielectric interface, i.e., one dimensional metallic grating, is described as $z = s(x)$ with period of a. The interface consists of dielectric with dielectric constant ε_{D} in the region $z > s(x)$ and metal in the region $z < s(x)$. The metal is characterized by a real, isotropic, and frequency dielectric function $\varepsilon_{\mathrm{D}}(\omega)$.

When SPP wave propagates on such a periodic interface, two standing wave solutions of SPP modes can be found with respect to the peaks and troughs of the interface. Therefore, the dispersion curve splits into two branches. Just like "photonic band gap" (PBG) in spatially periodic dielectric structures called "photonic crystals" [23]–[25], SPPBG can also occur, where propagation of SPP mode over certain range of frequency is forbidden [25]. At the BE-frequency, the density of state (DOS) for photon is very large and the SE rate can be greatly enhanced [11]–[15]. Since the BE-frequency only depends on the parameters of the metallic grating (period, depth, etc.), large DOS and SE rate enhancement can be achieved within a large frequency range by properly engineering the periodic structure in spite of the applied materials. In other words, the mismatch between surface plasmon frequency and luminescence frequency of Si-NCs can be overcome by adopting the metallic grating.

Our objective is to evaluate SE rate enhancement with such periodic structure as shown in Fig. 1. To achieve it, there are two steps. The first is to find the SPP modes solutions that satisfy the Maxwell's equations and the boundary condition. After both the dispersion relation $k(\omega)$ and the electromagnetic field distribution $\boldsymbol{E}(x,z)$ are obtained, the SE can be deduced from Fermi's Golden Rule and the Purcell factor (PF) can be calculated in success.

B. A Combination Method for SPP Mode Solution

In this section, we will introduce a combination method to obtain the numerical solution of SPP mode propagating on a cylindrical periodic dielectric-metal interface, including both of dispersion relation and field distribution. The proposed method is taking the advantages of the Green' function method (GFM) based on Rayleigh expansion [26], [27] and Chandezon's approach (CDA) for constructing the electromagnetic field distribution in two-dimensional expansion form [26], [27]. The details about the proposed method can be found in our previous work [22] and here only several important stages are presented.

Since the SPP mode is transverse magnetic (TM or p-polarized) wave, we are only interested in the TM solution of Maxwell's equations. In our reference coordinate system shown in Fig. 1, the magnetic field of SPP mode contains the field components perpendicular to the symmetry plane, i.e., the y component. Since the interface is uniform along y axis, the magnetic field will also be symmetrical along y axis and can be written as:

$$\overrightarrow{H}(x,y,z|\omega) = \overrightarrow{y} \cdot H_y(x,z|\omega)\exp(-i\omega t) \tag{1}$$

To find the SPP mode solution in x direction across the interface $z = s(x)$ and also whose amplitudes decay exponentially along the z direction, the process consists of calculating the dispersion relation with GFM and calculating field distribution with CDA.

According to GFM, the SPP mode solution can be deduced from the Helmholtz equations by using (1) and Maxwell's equations, then expanded as Fourier sums that possess the Bloch periodicity property as [26], [27]:

$$H_y(x,z|\omega) = \sum_{n=-\infty}^{+\infty} A_n \exp(i\beta_n z)\exp[i(k_x + nK_g)x] \tag{2}$$

Where k_x and A_n are the SPP mode wave vector in x direction and field expansion coefficients, respectively. $K_g = 2\pi/a$ is the Bragg wave vector of the interface. A series of wave vectors of SPP mode β_n are given by:

$$\beta_n = \left[(k_x + nK_g)^2 - \varepsilon\frac{\omega^2}{c^2}\right]^{1/2} \tag{3}$$

Here, $\varepsilon = \begin{cases}\varepsilon_D, z > s(x)\\ \varepsilon_M(\omega), z < s(x)\end{cases}$ and $H_y = \begin{cases}H_y^D, z > s(x)\\ H_y^M, z < s(x)\end{cases}$ represent the dielectric permittivity and magnetic filed in the appropriate medium (metal and dielectric), respectively. The metal is characterized by a real, isotropic, and frequency dependent dielectric function $\varepsilon_M(\omega)$.

The boundary conditions are satisfied by assuming that the expressions for the fields in the two half spaces are valid all the way to the interface, which is the Rayleigh hypothesis and such expansion of (2) is also called Rayleigh expansion.

By adopting the Green's second integral theorem, the problem can be simplified by working only with the field in the dielectric and a set of integral equations satisfied by the coefficients $\{A_n\}$ can be obtained:

$$\sum_n \frac{k_m k_n + \beta_m^M \cdot \beta_n^D}{i\left(\beta_m^M - \beta_n^D\right)} \cdot \frac{1}{a}\int_0^a dx \cdot \exp\left[-i\frac{2\pi}{a}(m-n)x\right] \times \exp\left\{i\left[\beta_m^M - \beta_n^D\right]\cdot s(x)\right\}\cdot A_n = 0 \qquad m = 0, \pm1, \pm2, \ldots \tag{4}$$

Where β_m^M and β_m^D represent the SPP mode wave vector in dielectric and metal, respectively.

For numerical calculation, (4) need to be truncated to finite term, i.e., given from $m, n = 0, \pm1, \pm2, \ldots$ and can be presented as a matrix multiplying a column vector:

$$[M_{m,n}(\omega, k_x, \varepsilon_D, \varepsilon_M, s(x))] \cdot [A_n] = 0 \tag{5}$$

In (5), the elements of coefficients matrix $[M_{m,n}]$ is related to the frequency ω and wave vector k_x of the SPP mode so that the dispersion relation $k_x(\omega)$ can be calculated by equating to zero the determinant of $[M_{m,n}]$ [26], [27].

After $k_x(\omega)$ is obtained, the next problem is to calculate the electromagnetic field distribution. In principle, field distribution could be obtained by calculating A_n expansion coefficients A_n while substituting the value of ω and k_x into the (5). However, it is very difficult to obtain exact value of ω and k_x to satisfy $\det[M] = 0$ in practical numerical calculation process. Matrix $[M]$ is an ill-conditioned matrix and the absolute value of each element in $[M]$ is quite different so that the exact valued of $|\det[M]| = 0$ is hard to be obtained. The detailed discussion can be found in our previous paper [22]. Such result indicates that GFM is not suitable to calculate the field distribution. To solve this problem, we expand the SPP mode solution according to CDA rather than Rayleigh expansion so that a new set of equations, different from (5), could be used to solve the electromagnetic field distribution under the known dispersion relation.

According to CDA, which is based on a coordinate transformation technique to make the interface flat, the SPP mode solution can be expanded in a two-dimensional expansion form [26]:

$$H_y(x,z) = \frac{1}{Z_0}\sum_m\sum_q f_m^q \times \exp\left[i\lambda^q(z - s(x))\right]\exp\left[i\left(k + m\frac{2\pi}{a}\right)x\right] \tag{6}$$

Where λ^q is the eigenvalues of the mode and f_m^q is the amplitude of the m th Fourier component of the H_y field in the q th eigenmode.

From (6), it can be easily found that the mode solution contains the shape information of the interface not only in the term of $\exp[i\lambda^q(z - s(x))]$ but also in the eigenvalues λ^q and coefficients f_m^q. This should be contrasted with the mode solution form in GFM, (2) (Rayleigh expansion), where the equivalent of the eigenvalues (wave vectors) $\beta_n = [(k_x + n\cdot K_g)^2 - \varepsilon\cdot(\omega/c)^2]^{1/2}$ are independent on the surface profile. Thus, the terms of Fourier summation to evaluate the relevant fields based on CDA are fewer than those based on Rayleigh expansion, i.e., GFM [29]. Furthermore, the SPP mode solution of CDA is very insensitive to the accuracy of the dispersion relation due to two-dimensional expansion form of the electromagnetic field [22]. In a word, CDA is more superior for constructing the electromagnetic field distribution. Taking the advantages of GFM and CDA, a convenient method to obtain the full SPP mode solution is proposed as follows:

1) Use the rectangle coordinate system x, y, z and calculate the coefficient matrix $[M]$ as (4)
2) Fix wave vector k, vary frequency ω with small step and look for changes in the sign of $\det[M]$. Then record the relation of $k \sim \omega$.
3) Transform coordinate system from x, y, z to $u = z - s(x), v = y, w = z$. For TM polarization mode, the component of the electric field locally parallels to the surface $E_{//}$ and that of the magnetic field normal to the symmetry H_y are re-expressed as:

$$F = \left(\frac{\mu_0}{\varepsilon_0}\right)^{1/2} H_y, G = -\frac{\omega}{c}\varepsilon E_{//}\sqrt{1 + s'^2} \tag{7}$$

Then a system of partial differential equations can be derived from the Maxwell's equations in covariant form and the Floquet–Bloch theorem:

$$-i\frac{d\xi}{du} = [T]\xi(u) \tag{8}$$

Where

$$\xi(u) = \lim_{N\to\infty}(F_{-N}, F_{-N+1}, \ldots, F_{N-1}, F_N, G_{-N}/\varepsilon, \ldots, G_N/\varepsilon)$$

is a generalized column vector. The coefficient matrix $[T]$ is also defined by the limit $N \to \infty$ of several assistant matrices and the detailed expression can be found in [28].

4) Substitute the relation of $\omega \sim k$ into coefficient matrix $[T]$ for each medium and calculate the eigenvalues λ^q and eigenvectors ϕ^q from $([T] - \lambda^q[I])[\phi^q] = 0$.

5) Calculate the expansion coefficients ξ_q in (8). coefficients ξ_q are proportional to the eigenvectors ϕ^q:

$$[\xi_q] = b_q[\phi_q] \tag{9}$$

Since the $\xi(u)$ is continuous at the boundary so that the proportional coefficient b_q in each medium can be calculated by a set of linear algebraic equations.

$$[\Phi^M][b^M] = [\Phi^D][b^D] \tag{10}$$

Where $[\Phi^j]\ j = M, D$ is a matrix whose columns are the eigenvectors ϕ^q and $[b^j]\ j = M, D$ is a column vectors of proportional coefficient b_q the in the appropriate medium (metal and dielectric).

6) Calculate the coefficients for electromagnetic field component $E_{//}$ and H_y. In order to obtain the field solution, we can write $[\xi_q] = [\begin{smallmatrix} f_m^q \\ g_m^q \end{smallmatrix}]$ and further convert the mode solution back to the rectangular coordinate system to obtain (6) and the mode solution for electronic field:

$$E_{//}(x,z) = -\frac{c}{\omega \cdot \varepsilon \cdot \sqrt{1+s'^2}} \cdot \sum_m \sum_q g_m^q \exp[i\lambda^q(z - s(x))] \exp\left[i\left(k + m\frac{2\pi}{a}\right)x\right] \tag{11}$$

7) By Maxwell's equations, the component of electric field locally normal to the surface E_N can be calculated as:

$$E_N(x,z) = \frac{1}{\omega \cdot \varepsilon \cdot \sqrt{1+s'^2}} \frac{\partial H_y}{\partial y} \tag{12}$$

The components of electric field along x and z direction, E_x and E_z, can be calculated as:

$$E_x(x,z) = -\frac{i \cdot c}{\omega \cdot \varepsilon} \cdot \frac{\partial H_y}{\partial z} \tag{13a}$$

$$E_z(x,z) = \frac{i \cdot c}{\omega \cdot \varepsilon} \cdot \frac{\partial H_y}{\partial x} \tag{13b}$$

Therefore, a combination method to solve the normal SPP mode propagating on a cylindrical periodic dielectric-metal interface is set up by taking the advantages of GFM and CDA.

C. Expression of Purcell Factor for Metallic Grating

After the dispersion relation $k_x(\omega)$ and the electromagnetic field distribution of SPP mode $\boldsymbol{E}(x,z)$ are obtained by the combination method proposed in Section II.B, the SE rate $\Gamma_{\rm sp}$ can be deduced from Fermi's Golden Rule:

$$\Gamma_{\rm sp} = \frac{2\pi}{\hbar}|\langle f|\boldsymbol{d}\cdot\boldsymbol{E}|i\rangle|^2\rho(\omega) \tag{14}$$

Where $\langle f|\boldsymbol{d}\cdot\boldsymbol{E}|i\rangle$ is the dipole emission matrix element, $\boldsymbol{d}$ is the electro-hole pair dipole moment, and $\rho(\omega)$ is DOS for photon. To evaluate $\Gamma_{sp}, \boldsymbol{E}$ should be normalized to a half-quantum of zero point fluctuations. Similar to the process in [11], the electrical filed is assumed to exist in a prepared space $V = L_x \cdot L_y \cdot L_z$, then the normalized electrical field can be expressed as:

$$E^2(x,z) = \frac{\hbar\omega/2}{1/8\pi \int^{L_x}\int^{L_y}\int^{L_z}[\partial(\varepsilon\omega)/\partial\omega]\cdot E_0^2(x,z)d_x d_y d_z} \cdot E_0^2(x,z) \tag{15}$$

Where $E_0(x,z)$ is the original field distribution. For SPP mode, the amplitudes decay exponentially along z direction so that the electrical field integration along z direction should be extended to $L_z \to \pm\infty$. While in x direction, the integration can re-expressed as $\int_0^{L_x} dx = (L_x)/(a)\int_0^a dx$ due to the periodic electrical field distribution $E_0(x+a,z) = E_0(x,z)$. Additionally, $\boldsymbol{E}(x,z)$ is homogeneous along y direction so that the term of stored energy can be expressed as $(1)/(8\pi)\cdot(L_xL_y)/(a)\int_0^a\int_{-\infty}^{+\infty}[\partial(\varepsilon\omega)/\partial\omega]E_0^2(x,z)dzdx$.

In the considered case, $k_x = k, k_y = 0$, which is a line in the space of wave vector, the DOS can be presented as:

$$\rho(\hbar\omega) = \frac{L_x}{2\pi}\cdot\frac{dk_x}{d(\hbar\omega)} \tag{16}$$

By (14)–(16), $\Gamma_{\rm sp}$ can be deduced as:

$$\Gamma_{\rm sp}(x,z) = \frac{4\pi\cdot\omega E_0(x,z)^2 d^2}{3\cdot\frac{L_y}{a}\cdot\int_0^a\int_{-\infty}^{+\infty}[\partial(\varepsilon\omega)/\partial\omega]E_0^2(x,z)dzdx} \cdot\frac{dk}{d(\hbar\omega)} \tag{17}$$

The polarization of electro-hole pair dipole moment is considered as random directional to that of electrical filed, averaged factor of 1/3 is taken for $|\langle\boldsymbol{d}\cdot\boldsymbol{E}\rangle|^2 = (1)/(3)d^2\cdot|E|^2$ [11].

By using (17) with well known SE rate in bulk semiconductor material [30], the Purcell factor can be expressed as:

$$\mathrm{PF}(x,z) = 1 + \frac{\pi c^3 E_0(x,z)^2}{n_r\cdot\omega^2\frac{1}{a}\cdot\int_0^a\int_{-\infty}^{+\infty}[\partial(\varepsilon\omega)/\partial\omega]E_0^2(x,z)dzdx} \cdot\frac{dk_x}{d\omega}\cdot\frac{1}{L_y} \tag{18}$$

Where n_r is the refractive index of the dielectric. In (18), it should be noticed that PF is related to L_y, the width along y axis, which denotes the width of the grating bar in a real waveguide. It is the result of that $\boldsymbol{E}(x,z)$ is treated as uniformity along y direction. In principle, it is strictly valid only while $L_y \to \infty$. However, the width of a real grating is always a limited value. So $L_y \gg \lambda_{\rm spp}/2$ could be taken as an approximation where $\lambda_{\rm spp}$ is the wavelength of considered SPP wave. As our experience, L_y could be considered large enough when $L_y > 3\lambda_{\rm spp}$ since a large portion of $\boldsymbol{E}(x,z)$ is constant. In this case, all wave vectors in the $k_x - k_y$ plane should be sum up for calculating DOS, which is a ring in the wave vector space as shown in [11], rather than a line segment of one dimensional DOS as in (16). In fact, the most significant SPPBG effect occurs in the mode of $k_x = k, k_y = 0$. For example, considering a special case of $k_x = 0, k_y = k$, the dispersion curve of SPP wave is similar to that of flat metal-dielectric surface with the

plasmon frequency much higher than the frequency range of Si-NCs luminescence, the frequency of such propagating SPP mode is much lower than the plasmon frequency, therefore the DOS of such mode would be much lower than that of $k_x = k, k_y = 0$ mode at the same frequency. In this work, our interest are focused on the SPP enhancement due to SPPBG so that only the mode of $k_x = k, k_y = 0$ was investigated. The full analysis about the two-dimensional case is still undergoing now and will be published elsewhere in the future. For the case of reducing the L_y will be discussed briefly in Section IV.B.

Till now, a full theoretical approach has been proposed and demonstrated to obtain the numerical solution of SPP mode propagating on metallic grating and related PF ((18)). In the followed section, the calculation results based on periodic Cu-Si_3N_4 interface will be discussed.

III. Results for Copper Grating

In the calculation, we assume that the Si-NCs are embedded in silicon nitride (Si_3N_4). Here Si_3N_4 was adopted because it is more promising to realize electroluminescence devices due to its lower barrier for electros and holes [31]. The permittivity of Si_3N_4 is assumed as $\varepsilon_D = 4$ while the dielectric function of Cu is obtained by the data reported in [32]. The metallic grating was assumed as sinusoidal shape $s(x) = h \cdot \sin(2\pi/a \cdot x)$ with period a and depth $h = 0.1\ a$.

A. Dispersion Curve

Firstly, the period was set as $a = 120$ nm. The order of coefficient matrix $[M_{m,n}]$ was set as 11 ($N = 5$) and the frequency searching step was set as $\omega_{\text{step}} = 10^{-4}$ eV. Then the dispersion curve can be calculated following the step1–2 described in Section II.B and the results are shown in Fig. 2. As a reference, the dielectric light line (Si_3N_4) and dispersion curve of flat Cu-Si_3N_4 interface are also plotted with dashed and solid line, respectively. The energy bandgap can be observed clearly. There are two branches for the dispersion curves of sinusoidal shaped interface while one is higher than that of flat interface and the other is lower. Moreover, the BE frequencies of SPP modes at the first Brillouin zone boundary ($k_x = K_g/2 = 2.62 \times 10^7$ m^{-1}) are also calculated by using analytical formulation in [29] and shown as hollow diamond in Fig. 2.

As expectation, the results of the numerical and analytical solutions are consistent. For the lower and higher frequency branches, the BE-frequencies are $\hbar\omega = 1.725$ eV and $\hbar\omega = 2.22$ eV, respectively, both which are lower than the plasmon frequency of flat Cu-Si_3N_4 interface ($\hbar\omega_{\text{spp}} = 2.855$ eV). In typical Si-NCs, the luminescent frequency is about $\hbar\omega = 1.6$–1.9 eV and the central frequency is $\hbar\omega = 1.72$ eV, which is nearly the same as the BE-frequency for lower branch.

Secondly, similar calculations are repeated while the period was varied from $a = 90$ to 140 nm. From the results shown in Fig. 3, it can be found that the BE-frequency for lower branch is varied from $\hbar\omega = 1.92$ to 1.58 eV with increasing period. Such results indicate that the BE-frequency of SPPBG can be engineered according to Si-NCs luminescence with proper grating period. Additionally, it should be noticed that there is only one branch for $a = 90$ nm. The reason is because the solutions for the higher branch are beyond the plasmon frequency ($\hbar\omega_{\text{spp}} = 2.855$ eV).

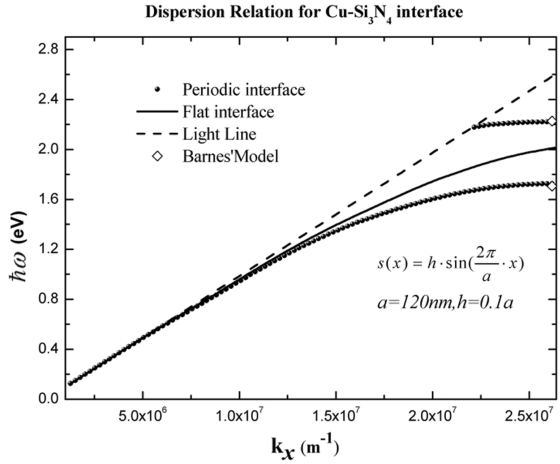

Fig. 2. Calculated dispersion curves for Cu-Si_3N_4 interface with sinusoidal shape (period $a = 120$ nm and depth $d = 12$ nm). Here the light lines in dielectric and dispersion curve of flat Cu-Si_3N_4 interface are also plotted with dashed and solid line, respectively. The BE frequencies of SPP modes at $k_x = K_g/2$ shown as hollow diamond are obtained by using analytical formulation in [29].

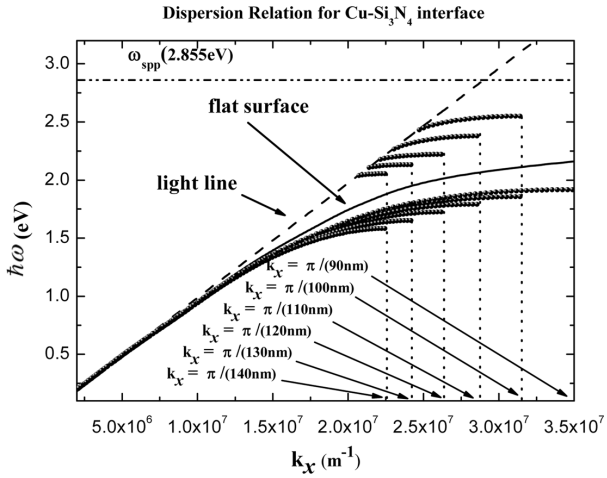

Fig. 3. Calculated dispersion curves for Cu-Si_3N_4 interface with sinusoidal shape with period $a = 90$–140 nm and depth $h = 0.1a$.

In principle, both the lower and higher branches could be applied for SPP enhancement. In Fig. 3, it can be observed that the lower branches are within the frequency range of Si-NCs while the higher branches are in the range of much higher frequencies. So if higher branches are desired for SPP enhancement, shorter grating wave vector (K_g) is required to move the dispersion curve of higher branch to short wave vector range. In Fig. 3, the dispersion curve of SPP mode on flat interface is much closer to the light line as decreasing wave vector. It could be expected that higher branches would be also very close to the light line due to the nature that higher branches are always between the dispersion curve on flat interface and dielectric light line. Intuitively, the achievable SPP enhancement of high branches would be very low. Furthermore, it can also be understood as that the wavelength of such SPP mode is much longer (shorter wave vector) so that the advantage introduced

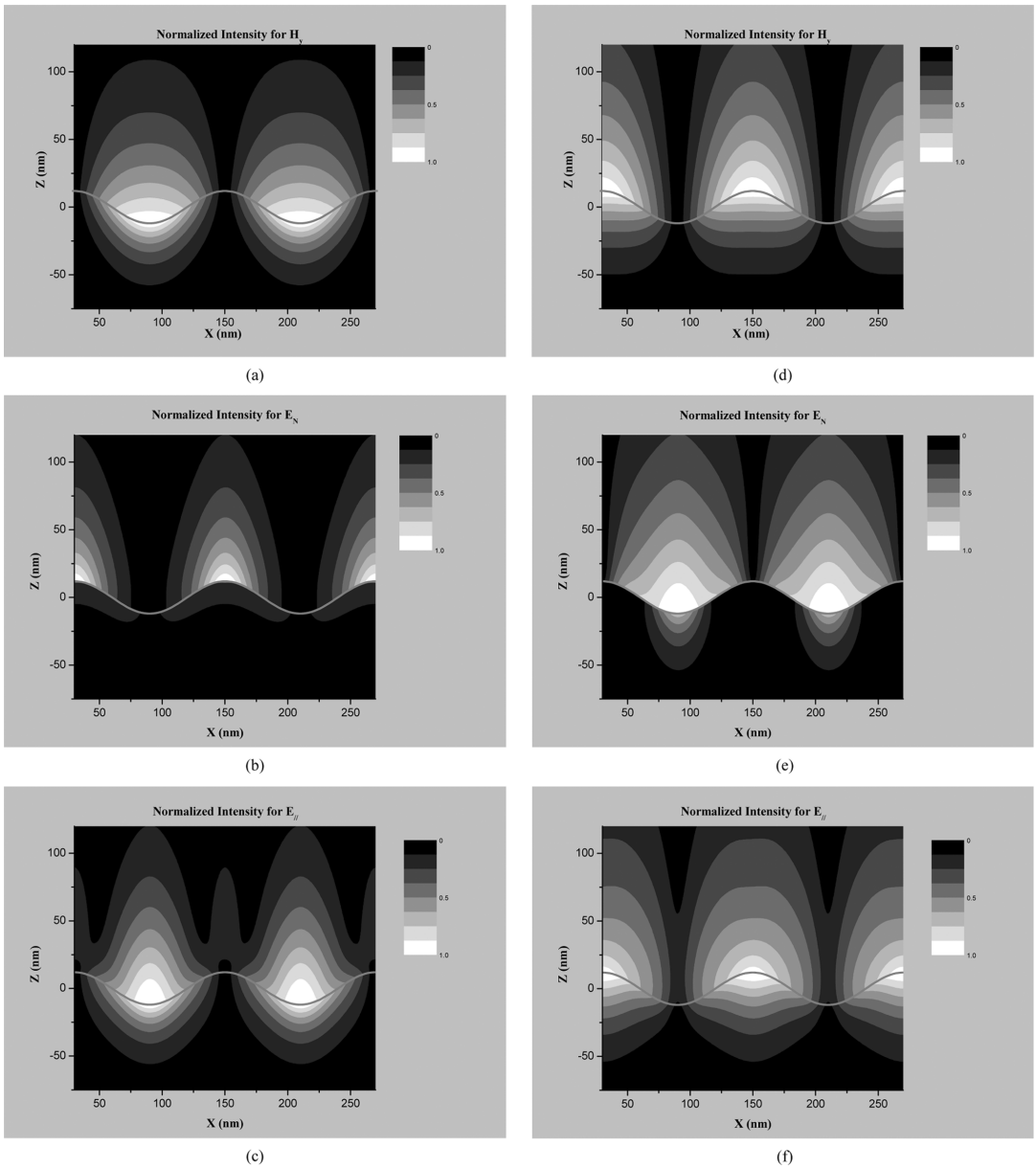

Fig. 4. Normalized spatial distribution of the magnetic field normal to the symmetry $|H_y|$ (a), electric field locally parallel to the surface $|E_{//}|$ (b) and normal to the surface $|E_N|$ (c) for low frequency mode and those for high frequency mode (d)–(f) at BE-frequency. The regions of high field strength are shown as white.

from small mode volume of SPP mode is not so significant. For this consideration, the lower branch is more preferred to be applied in the interested frequency range. It should be mentioned that the higher branches can also be applied if the semiconductor materials with higher luminescence frequency, e.g., blue light region such as GaN or Si-NCs with very small averaged size are considered.

B. Electromagnetic Field Distribution

Following the step 3–7 stated in Section II, the calculated dispersion curve was applied for calculating the electromagnetic field distribution based on CDA. Here the order of coefficient matrix $[T]$ was set as $5(N = 2)$ and the proportional coefficients b_q was obtained by solving (10) with least square method. The spatial region in calculation was divided to 401×401 mesh grids along x and z axis with the range of $a/4 \leq x \leq 2a + a/4$ and - $a \leq z \leq a$. With $a = 120$ nm, the field intensity of $H_y, E_{//}$, and E_N at BE-frequency were calculated and the results are shown in Fig. 4 in contour map, where all the intensity are normalized by the maximum value on boundary and the regions of high field strength are shown as white.

As mentioned by Barnes, the physical origin of the SPP bandgap can be found from the fact that two standing wave solutions of SPP modes take different positions with respect to the peaks and troughs of the interface [29]. Such indication can be observed clearly in Fig. 4. For the lower frequency mode, shown in Fig. 4(a)–(c), the surface charge distribution should be concentrated around the peaks so that extremum of normal field component, E_N, occur at the same position, whereas the extremum of H_y and is around the troughs. For the higher frequency mode shown in Fig. 4(d)–(f), E_N will occur at troughs.

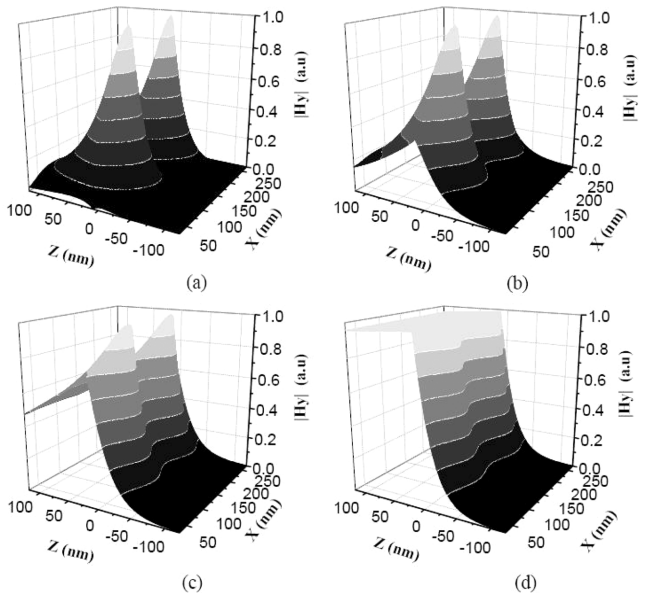

Fig. 5. Normalized field distributions of $|H_y|$ for the lower branch at $k_x = 0.5K_g$ (a), 0.38 K_g (b), 0.5 K_g (c), 0.05 K_g (d).

Furthermore, the field distribution at arbitrary wave vector can be obtained by substituting the wave vector k_x and related frequency ω on dispersion curve into the same calculating steps as shown in Section II.B. As an example, the field distributions at $k_x = 0.5K_g, 0.38K_g, 0.25K_g, 0.05K_g$ of the lower branch were calculated with the same conditions as Section III.A and the results of normalized $|H_y|$ are shown in Fig. 5(a)–(d). It can be observed that difference between the field strength at troughs and peaks of the interface decrease while reducing wave vector. When $k_x = 0.05K_g$, the curve is almost flat, which can observed more clearly from the $|H_y|$ distributions at interface as shown in Fig. 6. This fact can be easily understood as follows. At the BE-frequency, the two spatial waves propagating in opposite direction can perfectly interfere with each other so that standing wave distribution of SPP mode is generated. With the wave vector of SPP mode decreasing, only partial interference can occur and the field strength at troughs and peaks close up. When $k_x = 0.05K_g$, the wavelength of SPP mode is much longer than the period of interface so that the field distribution is nearly not affected by the interface corrugation and close to that on the flat metal-dielectric interface.

C. Calculation of Purcell Factor

After the field distribution at arbitrary wave vector are obtained, the PF with given grating parameters could be calculated with (18) in success. Fig. 7 is the calculated PF at BE-frequency for Cu-Si_3N_4 grating by setting $a = 120$ nm and $d = 0.1a$. The regions of high PFs are shown as white.

As shown in Fig. 7, PF is related to the position of Si-NCs along both x and z axis due to the localized electric field distribution. Especially, PF decays along z direction with $\boldsymbol{E}(x, z)$ so that significant SE enhancement can be achieved only when the Si-NCs are localized near the interface.

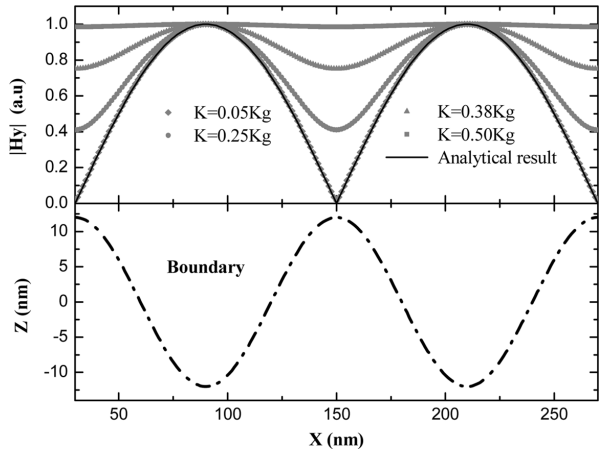

Fig. 6. The normalized field distributions of $|H_y|$ at interface for the lower branch at $k_x = 0.5K_g, 0.38K_g, 0.5K_g, 0.05K_g$. The solid line is for $k_x = 0.5K_g$ and calculated by using analytical formulation in [27].

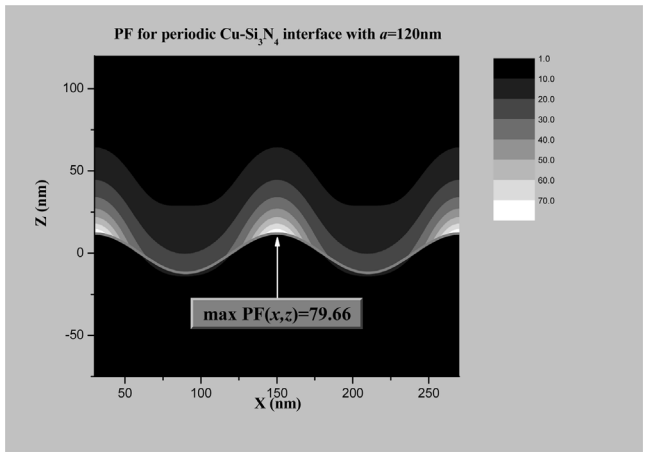

Fig. 7. Calculated PF distribution for Cu-Si_3N_4 grating within range of 30 nm $\leq x \leq 270$ nm and -120 nm $\leq z \leq 120$ nm by setting $a = 120$ nm and $d = 0.1a$. The regions of high PFs are shown as white.

In order to evaluate the SPP enhancement conveniently with various periods of grating, we assume that the Si-NCs are uniformly distributed in dielectric layer and the PF is averaged within one period along x axis and one decay length D_z along z axis, which denotes the length when the electric field decay to the 1/e of that at interface $z = s(x)$, in the dielectric:

$$\mathrm{PF}_{\mathrm{avg}} = \frac{1}{a} \cdot \frac{1}{D_z} \cdot \int_0^a \int_0^{D_z} \mathrm{PF}(x, z) dz dx \qquad (19)$$

Similar to that reported in [18], the averaged PF is used for discussion in the followed parts. Obviously, for a real device, D_z should be replaced by the thickness of the active layer. It should be mentioned that smaller D_z would be helpful to achieve larger PF since the Si-NCs are much closer to the interface. However, it also should be noticed that smaller D_z would lead to decreased quantity of Si-NCs. For example, when $D_y \to 0$, maximum PF $\mathrm{PF}(x, z = s(x))$ could be achieved since the Si-NCs are nearly localized at the interface while the quantity of Si-NCs would be close to zero. So it can be easily found that the total emission intensity would be very weak due to less Si-NCs even though large PF is obtained. So for optimizing the thickness of active

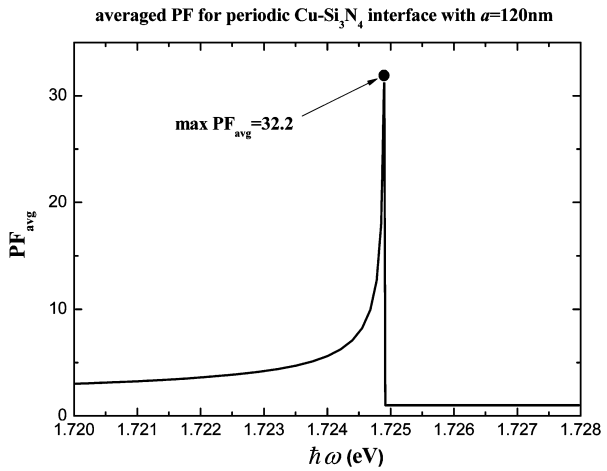

Fig. 8. Calculated $\mathrm{PF}_{\mathrm{avg}}$ at various frequency for Cu-Si_3N_4 grating with (19) by setting $a = 120$ nm and $d = 0.1a$.

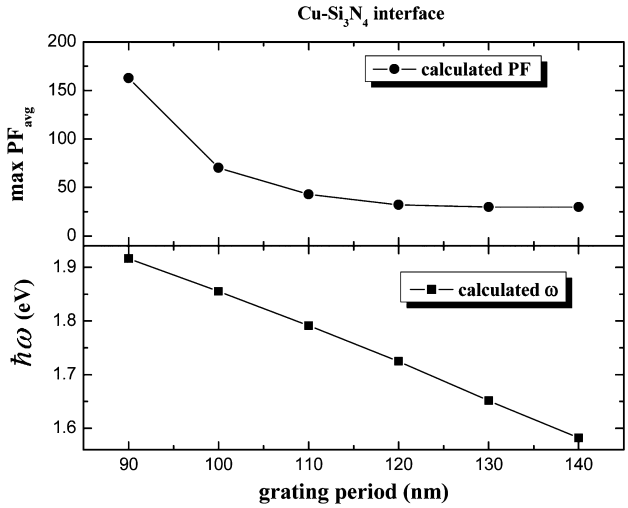

Fig. 9. Calculated max $\mathrm{PF}_{\mathrm{avg}}$ and related BE-frequency for Au-Si_3N_4 grating with grating period from 90 nm to 140 nm.

layer, there is a trade-off between larger SPP enhancement and more active Si-NCs. One possible solution is applying long and thin active Si-NCs layer.

With (19), the $\mathrm{PF}_{\mathrm{avg}}$ at various frequencies were obtained and shown in Fig. 8. As expected, the maximum $\mathrm{PF}_{\mathrm{avg}}$ of $\sim$32.2 is achieved at BE-frequency ($\hbar\omega = 1.725$ eV). When the frequency decreased to $\hbar\omega = 1.724$ eV, the PF is as low as 5.61. It can be understood intuitively that the DOS at BE-frequency is much larger than that at other frequency. Such result indicates that the enhancement occurs only in a narrow frequency range, which is very helpful to realize narrow band Si light source.

As shown in Fig. 3, the BE-frequency of SPPBG can be changed with varied grating period so that the related PF varies simultaneously. In Fig. 9, the calculated maximum value of $\mathrm{PF}_{\mathrm{avg}}(\max \mathrm{PF}_{\mathrm{avg}})$ and related BE-frequency are plotted versus the grating period. It can be seen that, as the period is varied from 90 to 140 nm, the BE-frequency decreased from $\hbar\omega = 1.92$ to 1.58 eV while the related max $\mathrm{PF}_{\mathrm{avg}}$ also decreased from 162.7 to 29.8. This is because that the original

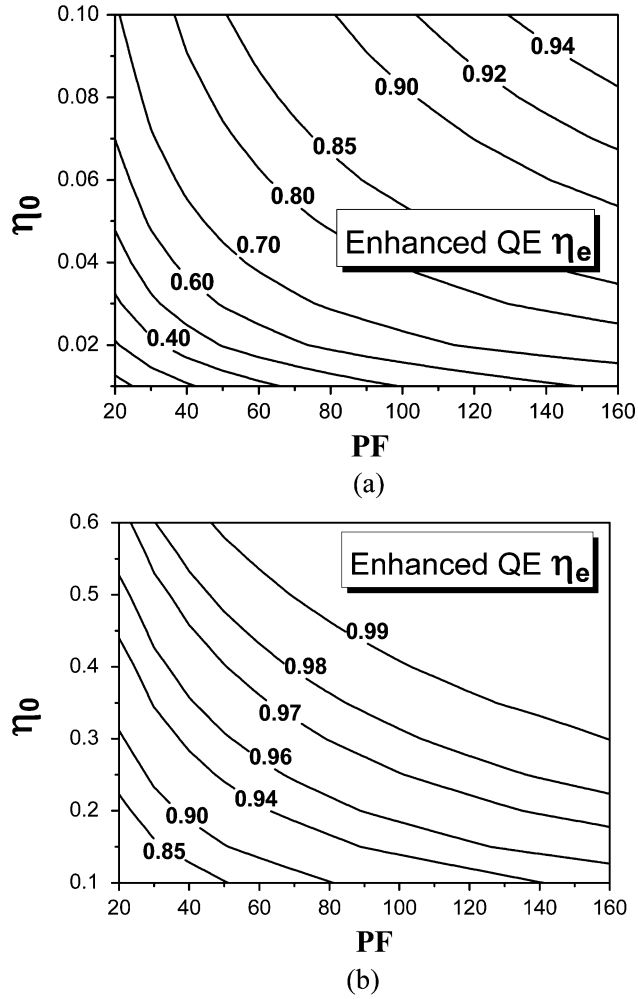

Fig. 10. The enhanced quantum efficiency $\boldsymbol{\eta_e}$ versus various PF and original quantum efficiency $\boldsymbol{\eta_o}$ for (a) $1\% < \boldsymbol{\eta_o} < 10\%$ and 10% $\boldsymbol{\eta_o} < 60\%$.

PF for flat Cu-Si_3N_4 is relatively higher in longer wave-vector range (closer to the plasmon frequency).

After the Purcell factor obtained, the enhanced quantum efficiency (QE) η_e can be evaluated from the original internal QE η_o :

$$\eta_e = \frac{\mathrm{PF}\cdot\tau_r^{-1}}{\mathrm{PF}\cdot\tau_r^{-1}+\tau_{\mathrm{nr}}^{-1}} = \eta_o\frac{\mathrm{PF}}{1+(\mathrm{PF}-1)\cdot\eta_o} \tag{20}$$

In (20), τ_r and τ_{nr} are the radiative and nonradiative lifetimes, respectively. The original QE η_o can be expressed as:

$$\eta_o = \frac{\tau_r^{-1}}{\tau_r^{-1}+\tau_{\mathrm{nr}}^{-1}} \tag{21}$$

With (20), the enhanced QE η_e are calculated in the range of $20 < \mathrm{PF} < 160$ and $1\% < \eta_o < 60\%$. For more clarity, the results for $1\% < \eta_o < 10\%$ and $10\% < \eta_o < 60\%$ are shown in Fig. 10(a) and (b), respectively.

From Fig. 10, significant QE improvement can be observed. In the lower η_o (1%–10%) range, the enhanced QE η_e can achieve the value of about 30%–94% as shown Fig. 10(a). For example, with setting $\eta_o = 3\%$ and $\mathrm{PF} = 40, \eta_e$ can be calculated as high as 55.3%. With higher (10%–60%), it is found that the η_e is very close to 100%. For example, with $\eta_o = 20\%$ and

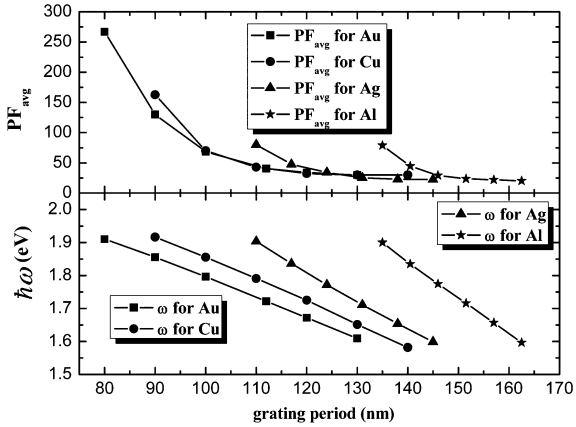

Fig. 11. The calculated max $\mathrm{PF}_{\mathrm{avg}}$ and related BE-frequency versus various period for sinusoidal shaped Au, Cu, Ag and Al-Si_3N_4 interface with $d = 0.1a$.

$\mathrm{PF} = 40$, the value of η_e is 91%. These results indicate that radiative recombination dominates over the active region, even with a very low original QE ($< 10\%$), which is not difficult to reach. However, the emission intensity of Si-NCs is much weaker than III-V semiconductor materials due to very long emission lifetime ($\sim$ ms) even though some of Si-NCs have very high internal QE values [20], [33], [34]. So such Si-NC materials are still not useful for practical emitters even with 30–163 folds of SPP enhancement and faster emission rates are required. In [35], fast radiative recombination in nitride-passivated Si-NCs is observed so that one can expect to improve the excitation densities and the emission rate of Si-NCs by new fabrication process. Since the PF is independent to the lifetime of Si-NCs, we believe that the SPP enhancement and Si-NCs with ultrafast luminescence will provide a promising approach to realize Si light emitter for optical interconnection on chip.

IV. Some Discussions

A. Comparing With Other Metal Gratings

In our previous work [19], it has been demonstrated that Au, Ag and Al-Si_3N_4 gratings can be used to enhance the SE of Si-NC with proper period. Since the same interface shape and depth/period ratio were adopted in [19] and this work, we re-plot the results for Au, Cu, Ag and Al in Fig. 11.

From Fig. 11, it can be seen that obvious enhancement are achieved within the frequency range of Si-NCs luminescence with the Au Cu, Ag and Al-Si_3N_4 grating. The SPP resonance frequencies for flat Au Cu, Ag and Al-Si_3N_4 interface are $\hbar\omega = 2.38$ eV, 2.85 eV, 3.15 eV and 6.92 eV, all of which are higher than the frequency of Si-NCs luminescence. Then it can be concluded that with proper setting grating period, metallic grating can be applied to overcome the mismatch between metal surface plasmon frequency and luminescence frequency of Si-NCs in spite of the applied metal materials. Meanwhile, it can be also found that both the BE-frequency and related max $\mathrm{PF}_{\mathrm{avg}}$ decreases as the period increased for all four cases. It could be understood that higher PF is achieved at high frequency since shorter period is corresponding to longer wave-vector and closer to the plasmon frequency. With the same reason, it is also can be understood why the shorter period and higher max $\mathrm{PF}_{\mathrm{avg}}$ can be achieved by such metal with relatively lower plasmon frequency.

Although all of the four kind metals can be employed to achieve plasmon-enhanced luminescence of Si-NCs with proper grating structure, one maybe want to know which is the best candidate for optical interconnection. Since Au and Ag are not compatible with silicon IC manufacturing while the achievable PFs of Al gratings are the lowest, it could be expected that Cu is more suitable to enhance the SE of Si emitters applied for optical interconnection.

B. How to Achieve Maximum Purcell Factor

As shown in (18) of Section II.C, the $\mathrm{PF}\ (x, z)$ is nearly proportioned to $1/L_y$, which is also consistent with the formula in [18]. It can be understood that L_y is in proportion to the mode volume of SPP mode, which is defined as

$$V = \left(\int_0^a \int_{-\infty}^{+\infty} [\partial(\varepsilon\omega)/\partial\omega] E_0^2(x,z)dzdx\right) / \left(\max\{[\partial(\varepsilon\omega)/\partial\omega] E_0^2(x,z)\}\right) \cdot L_y$$

[18], so that smaller mode volume and higher PF could be achieved by narrowing L_y.

For example, the maximum $\mathrm{PF}_{\mathrm{avg}}$ of–32.2 is achieved at BE-frequency ($\hbar\omega = 1.725$ eV) for Cu-Si_3N_4 interface with $L_y = 1$ μm while the value for $L_y = 10$ μm is only about 4.12. So the SE rate enhancement can be improved by reducing the width of grating bar in a real waveguide.

However, it should be noticed that the uniformity of SPP mode along y direction would be deteriorated when L_y is comparable to the wavelength of SPP wave. Then the approximation of $L_y \gg \lambda_{\mathrm{spp}}/2$, which is adopted in the above sections, is no longer valid. In such case, (18) would not give accurate estimation of the SPP enhancement and the wave vector along y axis (k_y) have to be taken into account. Considering the extreme case that wave vectors are uniform in the whole k_x-k_y plane, the related term can be calculated as $2k(dk)/(d\omega)$ by accounting all the wave vectors along the ring of $k_x^2 + k_y^2 = k^2$ in wave vector space as shown in [11]. For the mode of $k_x = k, k_y = 0$, investigated in this work, the term of $(dk_x)/(d\omega) \cdot (1)/(L_y)$ in (18) can be calculated as $(dk_x)/(d\omega) \cdot (1)/(3\lambda_{\mathrm{spp}}) = (k)/(6\pi) \cdot (dk)/(d\omega)$ by assuming $L_y = 3\lambda_{\mathrm{spp}}$ and $k_x = k = 2\pi/\lambda_{\mathrm{spp}}$. Comparing the value of $(k)/(6\pi) \cdot (dk)/(d\omega)$ and $2k(dk)/(d\omega)$, it can be expected that maximum SE enhancement could be achieved if the dispersion relations for any wave vector in the x-y plane are the same as that for k_x due to very large DOS.

So a certain waveguide or grating structure should be introduced to make the dispersion relation the same in both x and y direction, namely $k_y \sim \omega$ is as same as $k_x \sim \omega$ Therefore, the same SE enhancement can be achieved for the cases of both $k_x = k, k_y = 0$ and $k_x = 0, k_y = k$. Obviously, the most promising structure for such purpose is two dimensional periodic metal-dielectric interfaces and the main problem is how to design and realize the grating structure to achieve homogeneous dispersion relation in the whole x-y plane.

C. How to Extract Light From SPP Modes

In all of the sections, we have discussed the SE enhancement due to SPPBG on metallic-dielectric interface with the help of PF. With PF, how efficient the SE energy being coupled into SPP modes can be well evaluated. It is well known that the typical propagation distance of sub-wavelength SPP is tens of microns because metals are very absorptive in the visible and near-infrared [36]. So it should be considered that how to extract the SPP energy efficiently. It has been demonstrated that this purpose can be achieved by surface roughness [11] or metallic grating [13], [14], [18] to compensate the wave-vector mismatch between SPP mode and radiative mode. In [18], the measured enhancement ratio of photoluminescence emission was closely matched by theory, where biharmonic gratings were employed to establish SPPBG and extract the SPP mode simultaneously.

Unfortunately, it has been found that the overall SPP enhancement is limited by the ratio of coupling SPP mode into the continuum of radiation modes by a grating [13], [14]. It seems that the SPP enhancement does not offer any advantage for light emitting diode. However, such situation may be changed in some certain applications, e.g., optical interconnection, where it is more convenient to couple SPP mode into dielectric waveguide mode rather than radiation mode since optical waveguide is adopted to replace the copper line. In our recent work [37], the coupling performance between a short range SPP mode and a conventional dielectric waveguide mode was demonstrated. Typically, nearly all the energy of SPP mode can be coupled into waveguide mode within tens of microns [37]. At such case, the limitation of the SPP mode out-coupling efficiency may be overcome. Of course such indication should be confirmed and the related work will be reported elsewhere in the future. In this work, we neglect the propagation loss of SPP mode and only evaluate the SE enhancement by PF. Although such assumption would lead to divergence for evaluating the overall SPP enhancement of radiation efficiency in a real device, we believe that it does not influence the main point of this work that, by using SPPBG, the SE of Si-NCs can be enhanced by the metals with high surface plasmon frequency.

V. Conclusion

In conclusion, the SE rate enhancement due to SPPBG on Cu-Si_3N_4 grating was evaluated by calculating PF. With proper grating period, the BE-frequency of SPPBG can be engineered within luminescent frequency range of Si-NCs ($\hbar\omega = 1.6$–1.9 eV). The maximum PFs for Cu-Si_3N_4 gratings with 1 μm width are calculated as 29.8–162.7. These results indicate that the Cu grating can be employed to overcome the frequency mismatch between SPP resonance and Si-NCs luminescence. Since Cu is the most commonly adopted metal in integrated-circuit manufacturing, this work provide a promising approach to realize Si light emitter for optical interconnection on chip.

Furthermore, it was found that an effective way to improve the PF with constant grating period is reducing width of the grating bar. Following such consideration, we believe the most promising structure to achieve maximum PF is two dimensional metallic grating with homogeneous dispersion relation in the whole horizontal plane.

Acknowledgment

The authors would like to thank Xuan Tang, Weiwei Ke, Wei Zhang and Jiangde Peng for their valuable discussions and helpful comments.

References

[1] L. Pavesi, L. Dal Negro, C. Mazzoleni, G. Franzò, and F. Priolo, "Optical gain in silicon nanocrystals," *Nature*, vol. 408, pp. 440–444, 2000.

[2] K. D. Hirschman, L. Tsybeskov, S. P. Duttagupta, and P. M. Fauchet, "Silicon-based visible light-emitting devices integrated into microelectronic circuits," *Nature*, vol. 384, pp. 338–341, 1996.

[3] G. G. Qin and Y. J. Li, "Photoluminescence mechanism model for oxidized porous silicon and nanoscale-silicon-particle-embedded silicon oxide," *Phys. Rev. B*, vol. 68, pp. 085309–, 2003.

[4] D. Kovalev, H. Heckler, M. Ben-Chorin, G. Polisski, M. SchwartzkoPFf, and F. Koch, "Breakdown of the k-conservation rule in Si nanocrystals," *Phys. Rev. Lett.*, vol. 81, pp. 2803–2806, 1998.

[5] S. Godefroo, H. Hayne, M. Jivanescu, A. Stesmans, M. Zacharias, O. I. Lebedev, G. Van Tendeloo, and V. V. Moshschalkov, "Classification and control of the origin of photoluminescence from Si nanocrystals," *Nature Nanotechnology*, vol. 3, pp. 174–178, 2008.

[6] P. Bianucci, J. R. Rodríguez, C. M. Clements, J. G. C. Veinot, and A. Meldrum, "Silicon nanocrystal luminescence coupled to whispering gallery modes in optical fibers," *J. Appl. Phys.*, vol. 105, pp. 023108–, 2009.

[7] W. L. Wilson, P. F. Szajowski, and L. E. Brus, "Quantum confinement in size-selected surface-oxidised silicon nanocrystals," *Science*, vol. 262, pp. 1242–1244, 1993.

[8] A. G. Cullis and L. T. Canham, "Visible light emission due to quantum size effects in highly porous crystalline silicon," *Nature*, vol. 353, pp. 335–338, 1991.

[9] G. Franzò, F. Priolo, S. Coffa, A. Polman, and A. Carnera, "Room temperature electroluminescence from Er doped crystalline silicon," *Appl. Phys. Lett.*, vol. 64, pp. 2235–2237, 1994.

[10] H. S. Rong, A. Liu1, R. Jones, O. Cohen, D. Hak, R. Nicolaescu, A. Fang, and M. Paniccia, "An all-silicon Raman laser," *Nature*, vol. 433, pp. 292–294, 2005.

[11] I. Gontijo, M. Boroditsky, E. Yablonovitch, S. Keller, U. K. Mishra, and S. P. DenBaars, "Coupling of InGaN quantum-well photoluminescence to silver surface plasmons," *Phys. Rev. B*, vol. 60, pp. 11564–, 1999.

[12] K. Okamoto, I. Niki, A. Shvartser, Y. Narukawa, T. Mukai, and A. Scherer, "Surface-plasmon-enhanced light emitters based on InGaN quantum wells," *Nature Materials*, vol. 3, pp. 601–605, 2004.

[13] G. Sun, J. B. Khurgin, and R. A. Soref, "Practicable enhancement of spontaneous emission using surface plasmons," *Appl. Phys. Lett.*, vol. 90, pp. 111107–, 2007.

[14] J. B. Khurgin, G. Sun, and R. A. Soref, "Enhancement of luminescence efficiency using surface plasmon polaritons: Figures of merit," *J. Opt. Soc. Amer. B*, vol. 24, pp. 1968–1980, 2007.

[15] C. W. Lai, J. Au, and H. C. Ong, "Surface-plasmon-mediated emission from metal-capped ZnO thin film," *Appl. Phys. Lett.*, vol. 86, pp. 251105–, 2005.

[16] D. E. Chang, A. S. Sørensen, E. A. Demler, and M. D. Lukin, "Single-photon transistor using nanoscale surface plasmons," *Nature Phys.*, vol. 3, pp. 807–812, 2007.

[17] X. L. Hu, Y. D. Huang, W. Zhang, and J. D. Peng, "Dominating radiative recombination in a nanoporous silicon layer with a metal-rich Au $(1-\alpha)$-SiO_2 (α) cermet waveguide," *Appl. Phys. Lett.*, vol. 89, pp. 081112–, 2006.

[18] Y. Y. Gong, J. Lu, S. L. Cheng, Y. Nishi, and J. Vučković, "Plasmonic enhancement of emission from Si-nanocrystals," *Appl. Phys. Lett.*, vol. 94, p. 013106, 2009.

[19] X. Feng, F. Liu, and Y. D. Huang, "Calculated plasmonic enhancement of spontaneous emission from silicon nanoscrystals with metallic gratincs," *Opt. Commun.*, 2009, to be published.

[20] J. S. Biteen, D. Pacifici, N. S. Lewis, and H. A. Atwater, "Enhanced radiative emission rate and quantum efficiency in coupled silicon nanocrystal-nanostructured gold emitters," *Nano Lett.*, vol. 5, pp. 1768–1773, 2005.

[21] J. S. Biteen, L. A. Sweatlock, H. Mertens, N. S. Lewis, A. Polman, and H. A. Atwater, "Plasmon-enhanced photoluminescence of silicon quantum dots: Simulation and experiment," *J. Phys. Chem. C*, vol. 111, pp. 13372–13377, 2007.

[22] X. Feng, W. W. Ke, X. Tang, Y. D. Huang, W. Zhang, and J. D. Peng, "Numerical solution of surface plasmon polariton mode propagating on spatially periodic metal-dielectric interface," *J. Opt. Soc. Amer. B*, vol. 26, pp. B11–B20, 2009.
[23] E. Yablonovitch, "Inhibited spontaneous emission in solid-state physics and electronics," *Phys. Rev. Lett.*, vol. 58, pp. 2059–2062, 1987.
[24] S. John, "Strong localization of photons in certain disordered dielectric superlattices," *Phys. Rev. Lett.*, vol. 58, pp. 2486–2489, 1987.
[25] W. L. Barnes, S. C. Kitson, T. W. Preist, and J. R. Sambles, "Photonic surfaces for surface-plasmon polaritons," *J. Opt. Soc. Am. A*, vol. 14, pp. 1654–1661, 1997.
[26] A. V. Zayatsa, I. I. Smolyaninovb, and A. A. Maradudinc, "Nano-optics of surface plasmon polaritons," *Physics Reports*, vol. 408, pp. 131–314, 2005.
[27] B. Laks, D. L. Mills, and A. A. Maradudin, "Surface polaritons on large-amplitude gratings," *Phys. Rev. B*, vol. 23, pp. 4965–, 1981.
[28] J. Chandezon, M. T. Dupuis, and G. Cornet, "Multicoated gratings: A differential formalism application in the entire optical region," *J. Opt. Soc. Amer.*, vol. 72, pp. 839–, 1982.
[29] W. L. Barnes, T. W. Preist, S. C. Kitson, and J. R. Sambles, "Physical origin of photonic energy gaps in the propagation of surface plasmons on gratings," *Phys. Rev. B*, vol. 54, pp. 6227–, 1996.
[30] P. Milonni, *The Quantum Vacuum: An Introduction to Quantum Electrodynamics*. New York: Academic, 1994.
[31] N. M. Park, T. S. Kim, and S. J. Park, "Band gap engineering of amorphous silicon quantum dots for light-emitting diodes," *Appl. Phys. Lett.*, vol. 78, pp. 2575–, 2001.
[32] , M. J. Weber, Ed., *Handbook of Optical Materials*. Boca Raton, FL: CRC Press, 2003.
[33] M. L. Brongersma, P. G. Kik, A. Polman, K. S. Min, and H. A. Atwater, "Size-dependent electron–hole exchange interaction in Si nanocrystals," *Appl. Phys. Lett.*, vol. 76, pp. 351–, 2000.
[34] K. Okamoto, A. Scherer, and Y. Kawakami, "Surface plasmon enhanced light emission from semiconductor materials," *Phys. Stat. Sol. (c) 5*, vol. 824, pp. 2822–2824, 2008.
[35] H. Chen, J. H. Shin, P. M. Fauchet, J. Y. Sung, J. H. Shin, and G. Y. Sung, "Ultrafast photoluminescence dynamics of nitride-passivated silicon nanocrystals using the variable stripe length technique," *Appl. Phys. Lett.*, vol. 91, pp. 173121–, 2007.
[36] H. Raether, *Surface Plasmons on Smooth and Rough Surfaces and on Gratings*. Berlin: Springer-Verlag, 1988.
[37] R. Y. Wan, F. Liu, X. Tang, Y. D. Huang, and J. D. Peng, "Vertical coupling between short range surface plasmon polariton mode and dielectric waveguide mode," *Appl. Phys. Lett.*, vol. 94, p. 141104, 2009.

Xue Feng was born in Guizhou, China, in August 1977. He received the B.S., M.S., and Ph.D. degrees in electrical engineering from Tsinghua University in 1999, 2002, and 2005, respectively. Since 2005, he has been working as Assistant Professor in Department of Electronic Engineering, Tsinghua University, Beijing, China.

His major research interest has been in the area of optical communication, silicon light source and integrated devices based on surface plasmon polariton.

Fang Liu received the B.S. degree from Beijing Institute of Technology, Beijing, China, in 2003. He received the Ph.D. degree from the Department of Electrical Engineering, Tsinghua University, Beijing, in 2008.

His current research interest is in the area of surface plasmon polariton-based integrated optical devices and nanostructure optoelectronics.

Yidong Huang received the B.S. and Ph.D. degrees in optoelectronics from Tsinghua University, Beijing, China, in 1988 and 1994, respectively.

From 1991 to 1993, she was with Arai Laboratories, Tokyo Institute of Technology, Japan, on leave from Tsinghua University. She was with the Photonic and Wireless Devices Research Laboratories, NEC Corporation, from 1994 to 2003, where she was engaged in the research on semiconductor laser diodes for optical-fiber communication. In 2003, she joined the Department of Electronics Engineering, Tsinghua University, as a Professor. She is presently engaged in research on nanostructure optoelectronics.